

# Geophysical Research Letters



## RESEARCH LETTER

10.1029/2019GL083024

### Special Section:

Initial results of the ERG (Arase) project and multi-point observations in geospace

### Key Points:

- The first measurements of the conversion from equatorial noise to EMIC waves are presented
- Existence of  $M/Q = 2$  ions (deuteron or alpha particle) in the deep plasmasphere is essential to cause the conversion
- The ion composition ratio is quantitatively estimated in the deep plasmasphere using characteristics of the wave dispersion

### Supporting Information:

- Supporting Information S1
- Figure S1

### Correspondence to:

Y. Miyoshi,  
miyoshi@isee.nagoya-u.ac.jp

### Citation:

Miyoshi, Y., Matsuda, S., Kurita, S., Nomura, K., Keika, K., Shoji, M., et al. (2019). EMIC waves converted from equatorial noise due to  $M/Q = 2$  ions in the plasmasphere: Observations from Van Allen Probes and Arase. *Geophysical Research Letters*, 46. <https://doi.org/10.1029/2019GL083024>

Received 28 MAR 2019

Accepted 25 APR 2019

Accepted article online 29 APR 2019

## EMIC Waves Converted From Equatorial Noise Due to $M/Q = 2$ Ions in the Plasmasphere: Observations From Van Allen Probes and Arase

Y. Miyoshi<sup>1</sup> , S. Matsuda<sup>2</sup> , S. Kurita<sup>1</sup> , K. Nomura<sup>1</sup>, K. Keika<sup>3</sup> , M. Shoji<sup>1</sup> , N. Kitamura<sup>3</sup> , Y. Kasahara<sup>4</sup> , A. Matsuoka<sup>2</sup> , I. Shinohara<sup>2</sup> , K. Shiokawa<sup>1</sup> , S. Machida<sup>1</sup>, O. Santolik<sup>5,6</sup> , S. A. Boardsen<sup>7,8</sup> , R. B. Horne<sup>9</sup> , and J. F. Wygant<sup>10</sup>

<sup>1</sup>ISEE, Nagoya University, Nagoya, Japan, <sup>2</sup>ISAS/JAXA, Kanagawa, Japan, <sup>3</sup>Graduate School of Science, The University of Tokyo, Tokyo, Japan, <sup>4</sup>Graduate School of Natural Science and Technology, Kanazawa University, Kanazawa, Japan, <sup>5</sup>Department of Space Physics, Institute of Atmospheric Physics, The Czech Academy of Sciences, Prague, Czechia, <sup>6</sup>Faculty of Mathematics and Physics, Charles University, Prague, Czechia, <sup>7</sup>Goddard Planetary Heliophysics Institute, University of Maryland, Baltimore County, MD, USA, <sup>8</sup>Goddard Space Flight Center, NASA, Greenbelt, US, <sup>9</sup>British Antarctic Survey, Cambridge, UK, <sup>10</sup>School of Physics and Astronomy, University of Minnesota, Minneapolis, US

**Abstract** Equatorial noise (EN) emissions are observed inside and outside the plasmopause. EN emissions are referred to as magnetosonic mode waves. Using data from Van Allen Probes and Arase, we found conversion from EN emissions to electromagnetic ion cyclotron (EMIC) waves in the plasmasphere and in the topside ionosphere. A low-frequency part of EN emissions becomes EMIC waves through branch splitting of EN emissions, and the mode conversion from EN to EMIC waves occurs around the frequency of  $M/Q = 2$  (deuteron and/or alpha particles) cyclotron frequency. These processes result in plasmaspheric EMIC waves. We investigated the ion composition ratio by characteristic frequencies of EN emissions and EMIC waves and obtained ion composition ratios. We found that the maximum composition ratio of  $M/Q = 2$  ions is  $\sim 10\%$  below 3,000 km. The quantitative estimation of the ion composition will contribute to improving the plasma model of the deep plasmasphere and the topside ionosphere.

**Plain Language Summary** Equatorial noise (EN) emissions are whistler mode waves. Using Van Allen Probe and Arase (ERG) plasma wave data, we found that EN emissions propagate toward the Earth and are converted to electromagnetic ion cyclotron (EMIC) waves in the deep plasmasphere and the topside ionosphere. We suggest that minor ions with a mass per charge ( $M/Q$ ) = 2, that is, deuteron or alpha particles, play an important role in this process. The processes reported here are a new generation process of plasmaspheric EMIC waves. Moreover, we determined the ion composition ratio using characteristics of wave dispersion. We derived the altitude profile of the ion composition ratio and identified the maximum ratio of  $M/Q = 2$  ions of about 10% in the deep plasmasphere.

## 1. Introduction

Equatorial noise (EN) emissions (Gurnett, 1976; Russell et al., 1970) are often observed inside and outside the plasmopause. It should be noted that EN emissions are referred to as magnetosonic mode waves (Boardsen et al., 1992; Gul'elmi et al., 1975) and Rauch and Roux (1982) referred to this wave as the class-2 wave. EN emissions are generated through the ring distribution of the ring current protons (Ma et al., 2014; Min & Liu, 2015; Umeda et al., 2012). EN emissions are generated near the magnetic equator (e.g., Boardsen et al., 2016; Santolik et al., 2004) and propagate across the magnetic field lines (Ma et al., 2014). The waves propagate toward Earth inside the plasmasphere (Horne et al., 2000; Horne & Miyoshi, 2016; Xiao et al., 2015) and azimuthally around Earth (Kasahara et al., 1994) across the field lines without significant damping.

EN emissions typically have wave normal angles (WNA) within  $\pm 2^\circ$  of  $90^\circ$  (e.g., Boardsen et al., 2016); however, at frequencies less than  $f_{cP}$ , the spread can be much broader in WNA, and it is expected that the polarization of the waves changes from right-hand (RH) to left-hand (LH) polarized at the crossover frequency. The crossover frequency, where the refractive indices for the RH waves are equal to those of the LH waves, is given by

©2019. The Authors.

This is an open access article under the terms of the Creative Commons Attribution-NonCommercial-NoDerivs License, which permits use and distribution in any medium, provided the original work is properly cited, the use is non-commercial and no modifications or adaptations are made.

$$\frac{1}{\Omega_e^2} + \sum_i \frac{A_i}{\left(\frac{m_i}{m_e}\right)^2 \omega_{cr}^2 - \Omega_e^2} = 0 \quad (1)$$

where  $m_i$  and  $m_e$  are the masses of ion species  $i$  and electron, respectively.  $\Omega_e$  is the electron cyclotron frequency (Kimura, 1966). The cutoff frequency ( $\omega_{cut}$ ) of the LH is given by

$$\begin{aligned} 1 - \frac{X_e}{1 + Y_e} - \sum_i \frac{X_i}{1 - Y_i} &= 0 \\ X_e &= \frac{\omega_{pe}^2}{\omega_{cut}^2}, Y_e = \frac{\Omega_e}{\omega_{cut}} \\ X_i &= \frac{\omega_{pi}^2}{\omega_{cut}^2}, Y_i = \frac{\Omega_i}{\omega_{cut}} \end{aligned} \quad (2)$$

where  $\omega_{pe}$  and  $\omega_{pi}$  are the plasma frequency of the electrons and ions, respectively, and  $\Omega_i$  is the cyclotron frequency of the electrons and ions. The summation of relative composition ratio  $A_i$  should be 1.

$$\sum_i A_i = 1 \quad (3)$$

Considering that the local crossover frequency depends on the L-shell (Horne & Throne, 1993; Matsuda et al., 2016), it is expected that the RH polarization of EN emissions should readily change to LH polarization during its radial propagation toward Earth inside the plasmasphere (Parrot et al., 2016; Santolik & Parrot, 1999, 2000). In fact, Santolik et al. (2016) reported that the polarization reversal of the whistler is decoupled from the low-frequency magnetosonic branch at low-altitudes from the DEMETER observations. This is not the mode conversion but is the polarization reversal of EN emissions along the same wave branch.

In the deep plasmasphere, the existence of minor ions of mass per charge ( $M/Q$ ) = 2 (deuterons and/or alpha particles) is expected based on plasma wave observations (Watanabe & Ondoh, 1976; Matsuda et al., 2014a, 2014b, 2015, 2016), so we should consider the presence of  $M/Q = 2$  ions together with  $H^+$ ,  $O^+$ , and  $He^+$  ions. As shown later, four different electromagnetic ion cyclotron (EMIC) waves can exist under the presence of  $M/Q = 2$  ions as possible wave modes. If EN emissions propagate toward low altitudes, where the ratio of  $M/Q = 2$  ions will become larger, it is expected that the wave component below  $f_{cM/Q=2}$  (cyclotron frequency of  $M/Q = 2$  ions) becomes EMIC waves through branch splitting and that the mode conversion takes place around  $f_{cM/Q=2}$ . However, these processes between EN and EMIC waves have not been reported.

In this paper, we report on the mode conversion from EN emissions to EMIC waves in the deep plasmasphere based on Van Allen Probes and Arase (ERG) observations. The presence of  $M/Q = 2$  ions plays an indispensable role in the generation of the proton band EMIC waves through the mode conversion from EN emissions. We also investigate the ion composition ratio by the observed crossover and  $L = 0$  cutoff frequencies from the wave observations, and we quantitatively show the altitude profile of the ion composition ratio in the deep plasmasphere.

## 2. Analysis of Van Allen Probe and Arase Observations

In this study, we use data from the electric field and waves (EFW) instrument (Wygant et al., 2013) and search coil sensors for the Electric and Magnetic Field Instrument Suite and Integrated Science (Kletzing et al., 2013) on board the Van Allen Probe-A. We also use the waveform data from the wave form capture (WFC) of the Plasma Wave Experiment (Kasahara et al., 2018; Matsuda et al., 2018) on board the Arase (ERG) satellite (Miyoshi, Hori, et al., 2018; Miyoshi, Shinohara, et al., 2018). The Arase satellite has operated the wave burst observations intermittently to obtain the wave form with the sampling frequency of 1,024 Hz. The ambient magnetic field is observed by the Magnetic Field Experiment (MGF) on board the Arase satellite (Matsuoka et al., 2018). Typical EMIC waves observed by Arase are reported in Matsuda et al. (2018) and Shoji et al. (2018).

We investigate the wave spectrum, wave polarization, and wave propagation directions using the spectral matrix. The spectral matrix is estimated from the frequency analysis of the EFW waveform data. In this study, the singular value decomposition (SVD) method (Parrot et al., 2016; Santolik et al., 2003; Santolik

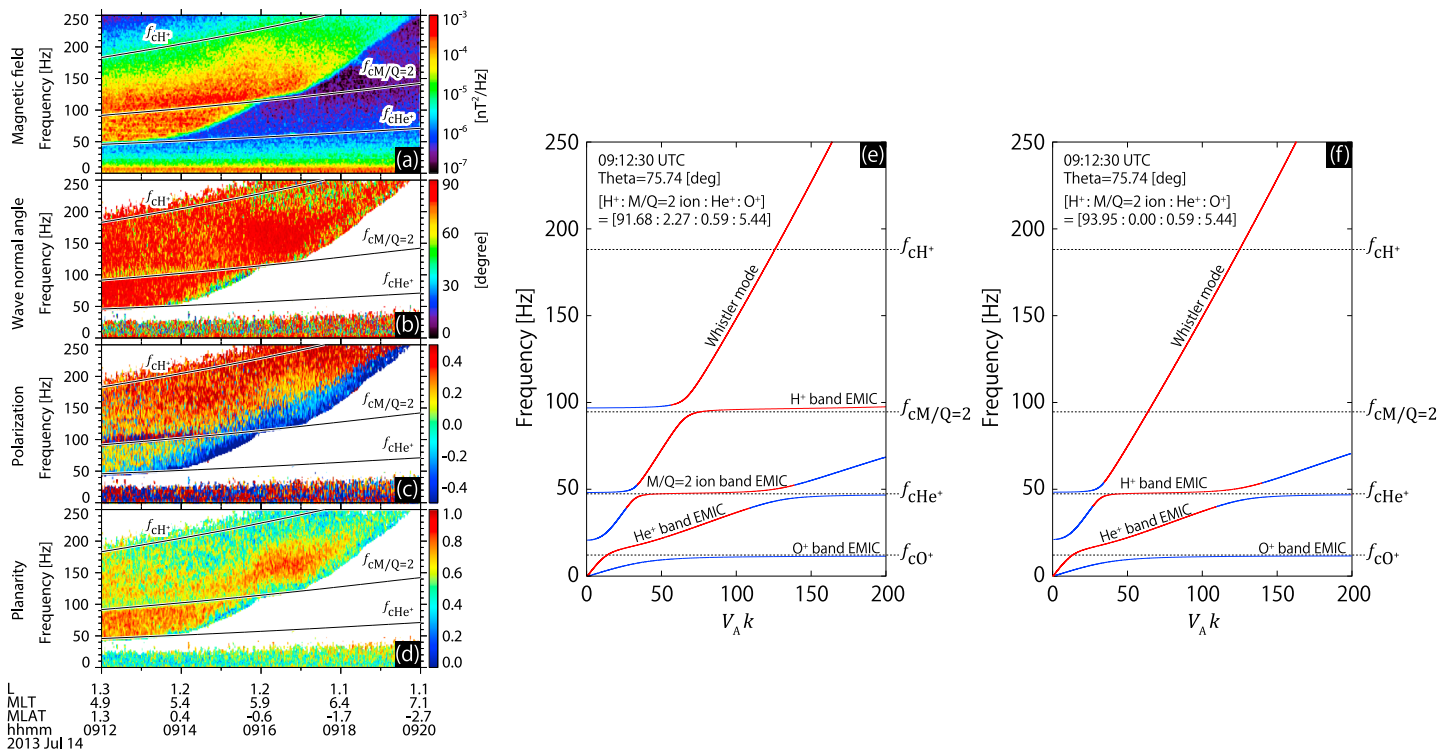


**Figure 1.** (a) Frequency-time diagram of magnetic field observed by EFW. The horizontal axis is time, and L and Magnetic Local Time (MLT) are taken along the satellite trajectory. (b) Same as (a) but the elevation angles of the wave normal vector are derived from the spectrum matrix. (c) Same as (a) but for wave polarization. The positive sign indicates right hand, while the negative sign indicates left hand. (d) Same as (a) but for wave planarity. Three black lines in the figures correspond to the local ion cyclotron frequency of H<sup>+</sup>, M/Q = 2 ions, and He<sup>+</sup> respectively. (e) Wave dispersion relations at 09:12:30 UTC. The horizontal axis is the product of the Alfvén velocity and wave number. The vertical axis is the frequency. The red color indicates right-hand polarization and blue left-hand polarization. (f) Same as (e) wave dispersion relations at 09:12:30 UTC but the ion composition of H<sup>+</sup>, O<sup>+</sup>, and He<sup>+</sup> are assumed. EMIC = electromagnetic ion cyclotron.

& Gurnett, 2002) is used to derive the wave propagation characteristics. The polarization, wave normal angles, and magnetic planarity are derived from the magnetic spectral matrix.

Figure 1a shows the frequency time diagram of magnetic fields obtained from the EFW that was observed on 14 July 2013. During that time, the Van Allen Probe traversed the plasmasphere and the topside ionosphere from ~3,200 to ~1,000 km (the corresponding Roeder L\* is 1.3 and 1.1, respectively). The three black lines correspond to the local cyclotron frequencies of H<sup>+</sup>, M/Q = 2 ions, and He<sup>+</sup>, respectively. The broadband emissions from 50 to ~250 Hz are EN emissions. Two cutoff frequencies can be found. The low-frequency cutoff started around 50 Hz at 09:12 UTC, and this cutoff frequency gradually increased when the satellite moved toward the lower L-shell. Another cutoff frequency is seen at approximately 90 Hz at 09:12 UTC, and this cutoff frequency also gradually increased.

Figure 1b shows the elevation angle of wave normal vectors relative to the ambient magnetic field, which indicates that a wave vector of EN is perpendicular to the ambient magnetic field. The analysis of wave vectors on the azimuthal angle (not shown) indicates that EN emissions propagate toward the earth during the period. Figure 1c shows the frequency-time diagram of the polarization derived from the SVD method. The red and blue indicate RH and LH, respectively, while the green indicates linear polarization. Looking at the polarization at 09:12 UTC, the polarization at a frequency above  $f_{cM/Q=2}$  is RH, while the polarization below  $f_{cM/Q=2}$  is almost linearly polarized. After 09:12 UTC, LH polarization is found at a frequency below  $f_{cM/Q=2}$ . After 09:15 UTC, only the LH polarization is seen at a frequency below  $f_{cM/Q=2}$ , and LH polarization is also seen above  $f_{cM/Q=2}$ . Figure 1d shows the frequency-time diagram of the planarity. During the period, the planarity is almost 1, which is a necessary condition for the plane wave assumption.

To specify the wave modes, we show the wave-dispersion relation. The wave-dispersion relation is derived from the following analysis. Since the wave power gap along  $f_{cM/Q=2}$  is observed, it is natural to consider multi-ion populations, including H<sup>+</sup>, M/Q = 2 ions, He<sup>+</sup> and O<sup>+</sup>. From Figure 1a and c, we can

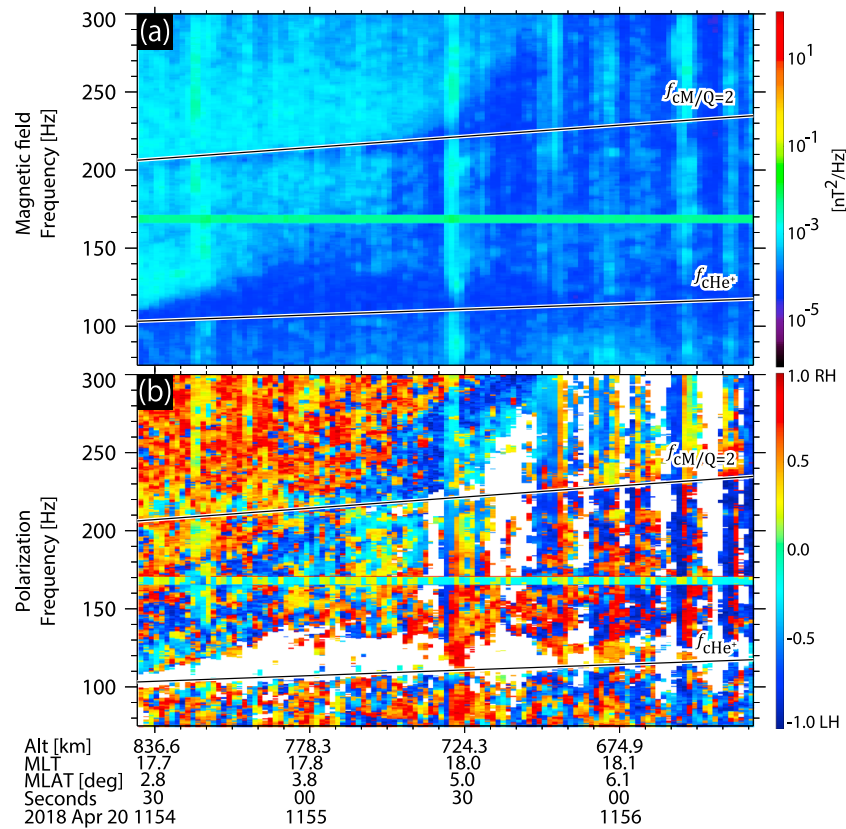


**Figure 2.** Conversion from equatorial noise emissions to electromagnetic ion cyclotron wave obtained by Arase Plasma Wave Experiment/wave form capture at low altitudes. The horizontal axis is time, and altitudes and MLT are taken along the satellite trajectory. (a) The frequency-time diagram of the magnetic field is obtained by Plasma Wave Experiment/wave form capture. The two black lines show the local ion cyclotron frequency of  $H^+$  and  $M/Q = 2$  ions. (b) Same as (a) but for wave polarization. The positive sign indicates right hand, while the negative sign indicates left hand. EMIC = electromagnetic ion cyclotron.

determine the crossover frequency between  $f_{cHe^+}$  and  $f_{cM/Q=2}$ , and two cutoff frequencies at a frequency above  $f_{cHe^+}$  and around  $f_{cM/Q=2}$ . Using these three characteristic frequencies, four different equations, that is, one equation on the crossover frequency (equation (1)), two equations on the cutoff (equation (2)) and equation (3) can be used to determine the ion composition ratio. The ambient plasma frequency ( $f_p$ ) and the local electron cyclotron frequency ( $f_{ce}$ ) are derived from the Van Allen Probe observations (Kurth et al., 2015). The estimated ion composition ratio of ( $H^+ : M/Q = 2$  ions:  $He^+ : O^+$ ) at 09:12:30UTC is ( $\sim 91.68\% : \sim 2.27\% : \sim 0.59\% : \sim 5.44\%$ ).

These ion composition ratios are used for the dispersion relation. Figure 1e is the wave-dispersion relation at 09:12:30 UTC. The wave normal angle is  $75.7^\circ$  at 100 Hz, which is used to calculate the wave-dispersion for the whole frequency range at this time. The estimated ion composition ratio is also considered. Five different branches are found, that is, whistler waves above  $f_{cM/Q=2}$ , proton band EMIC waves above  $f_{cHe^+}$ , the  $M/Q = 2$  ion,  $He^+$  band EMIC waves below  $f_{cHe^+}$ , and  $O^+$  band EMIC waves as the lowest frequency band.

In comparing Figure 1c with Figure 1e, we confirmed the wave modes that appeared in Figure 1c. The highest frequency components above  $f_{cM/Q=2}$  are EN emissions. Before 09:15 UTC, the polarization above  $f_{cM/Q=2}$  is almost RH, and it is difficult to find the crossover frequency because of the limited frequency resolution, although LH polarized waves are expected from theoretical investigations. After 09:15 UTC, both LH and RH polarized waves are found because of the increase of the crossover frequency at low altitudes. The frequency component between  $f_{cM/Q=2}$  and  $f_{cHe^+}$  is the proton band EMIC waves. Wide-band linear polarization and a narrow-band LH frequency range are seen at 09:12 UTC, and then polarization at a frequency

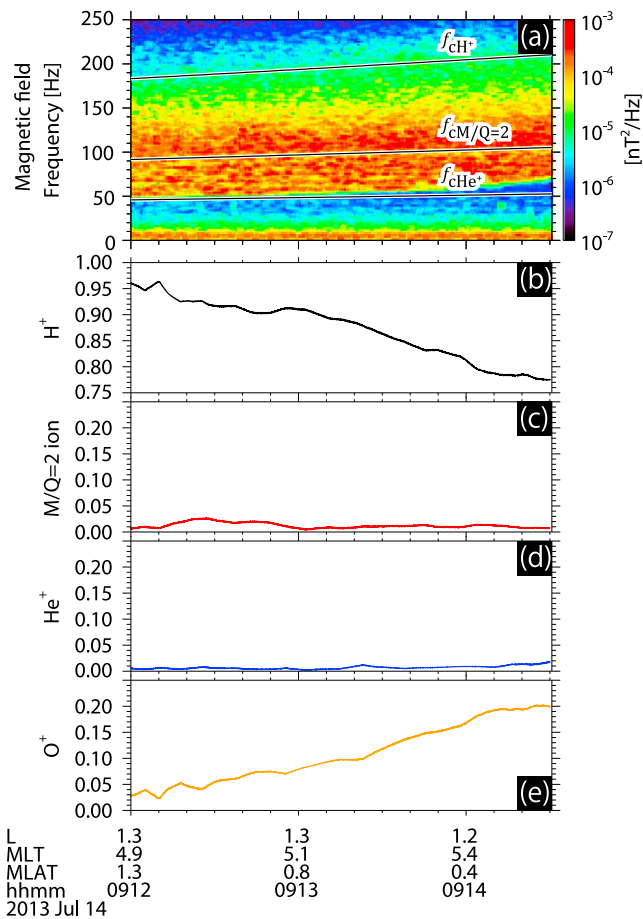


**Figure 3.** Example of equatorial noise emissions and electromagnetic ion cyclotron waves and the estimated ion composition ratio along the satellite orbit. (a) Same data format as Figure 1a; (b–e) the ion composition ratio estimated from wave observations:  $H^+$ ,  $M/Q = 2$  ions,  $He^+$ , and  $O^+$ , respectively.

below  $f_{cM/Q=2}$  changes to LH polarization due to the increase of crossover frequency. No significant waves are excited below  $f_{cHe^+}$ .

Here we focus on the frequency at 100 Hz. At 09:12 UTC, the waves at 100 Hz are EN emissions because the frequency is higher than the local  $f_{cM/Q=2}$ . The waves propagate to the lower altitudes and cross at the frequency of  $f_{cM/Q=2}$  at 09:13 UTC, when significant damping of wave power is detected, and then the wave mode at 100 Hz becomes the proton band EMIC waves with RH polarization. At 09:14:40, the polarization at 100 Hz changes from RH to LH, because the crossover frequency of the proton band EMIC waves increases at low altitudes. This result indicates that EN emissions (the whistler mode branch) split into EN emissions and proton band EMIC waves.

To consider the mode conversion from EN emissions to the proton band EMIC waves, we show another wave dispersion relation in Figure 1f. This dispersion relation is the same as that shown in Figure 1e, but  $M/Q = 2$  ions are not included. We assume that the proton composition ratio in Figure 1f is the sum of the composition ratios for both proton and  $M/Q = 2$  ions in Figure 1e. In Figure 1f, we see the whistler mode branch and the proton/helium/oxygen band EMIC waves, but we do not see any gap at the frequency around  $f_{cM/Q=2}$ . In comparing Figures 1e and 1f, the mode conversion occurs from a low-frequency component of the whistler (EN emissions) waves to  $H^+$  band EMIC waves through branch splitting due to the presence of  $M/Q = 2$  ions.

EN emissions and EMIC wave are also detected by the recent Arase satellite observations in the deep plasmasphere. Figure 2a shows the magnetic field spectra observed by Plasma Wave Experiment/WFC on board Arase on 20 April 2018. During this time, the Arase satellite observed EN emissions above 110 Hz in the altitude range from 830 to 670 km (the corresponding Roeder  $L^*$  are 1.03 and 1.01, respectively). The same polarization reversal as shown in Figure 1 is observed. There exists a cutoff of EN emissions along the local  $f_{cM/Q=2}$ . Figure 2b shows a frequency-time diagram of polarization estimated from the SVD method during the period. At 11:55 UTC, the polarization at frequencies

below the local  $f_{cM/Q=2}$  is LH; that is, the proton band EMIC waves. On the other hand, the polarization at frequencies above the local  $f_{cM/Q=2}$  is RH, that is, EN emissions. From both Van Allen Probes and Arase observations, we expect that the conversion from EN emissions to EMIC waves is common phenomena that occur at low altitudes, and we show the results from the statistical survey in section 3.

### 3. Investigation of the Ion Composition

As we have mentioned, using equations (1)–(3) for the dispersion relation, the relative abundance of each ion species can be estimated. Figure 3 is an example of the ion composition ratio estimated from Figure 1b. Figure 3a is similar to Figure 1a in data format. Figures 3b–3e show the estimated ratio of  $H^+$ ,  $M/Q = 2$  ions,  $He^+$ , and  $O^+$ , respectively. The ratio of the proton (oxygen) decreases (increases) when the satellite moves toward the low altitudes, and this is a typical altitudinal dependency of the ion composition. In addition to these ions, a few percent of  $M/Q = 2$  ions are expected during the period. The existence of  $M/Q = 2$  ions has been reported in previous research on plasma waves (Watanabe & Ondoh, 1976; Matsuda et al., 2014a, 2014b, 2015, 2016), while this is the first result reported for a quantitative estimate of the ion composition ratio.

From the survey of the EFW burst data from 26 January 2013 to 16 July 2016, we statistically investigate the ion composition ratio near Earth. The number of the burst mode operation near the perigee altitudes was 23, and we identified 12 events of the conversion. Considering the signal-to-noise ratio, we use eight events to estimate the ion composition.

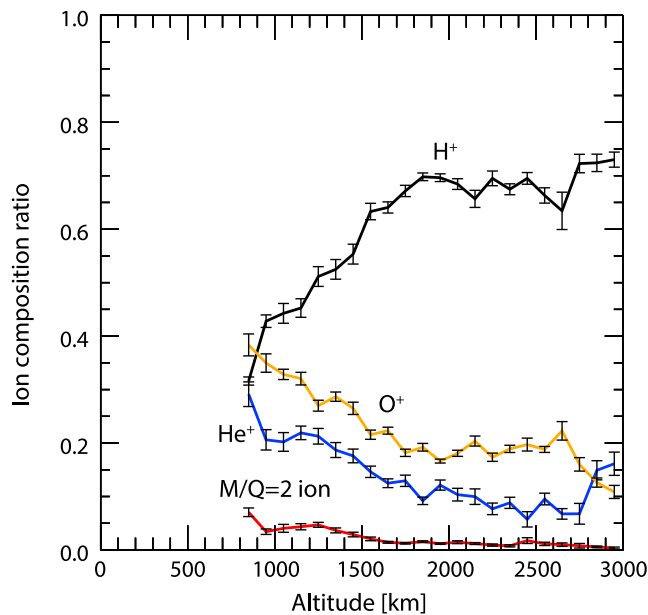


**Figure 4.** Altitude dependence of the estimated ion composition. The colors are the same as in Figure 3. The error bars indicate the standard deviation at each altitude.

Figure 4 shows the altitude profile of the ion composition up to 3,000 km, which was derived from the crossover frequencies and the cutoff frequencies. The black, blue, orange, and red indicate the ion composition ratio for  $H^+$ ,  $He^+$ ,  $O^+$ , and  $M/Q = 2$  ions, respectively. The proton abundance decreases sharply below 2,000 km, while the abundance of  $O^+$  increases.  $M/Q = 2$  ions exist at the lower altitudes, and the maximum ratio is  $\sim 10\%$  at the lowest altitude.

#### 4. Summary and Discussions

The conversion process shown in this study is a general linear mode conversion process in the multicomponent plasma. As shown in Figures 1e and 1f, the whistler wave branch should split into different wave modes, and a low-frequency component of the whistler waves into  $H^+$  band EMIC waves (Fraser, 1985). Branch splitting occurs due to the presence of  $M/Q = 2$  ions, and the new cutoff of EN emissions appears around  $f_{cM/Q=2}$ .

There are several origins of plasmaspheric EMIC waves (Kasahara et al., 1992; Sakaguchi et al., 2013; Sawada et al., 1991). Cyclotron resonance with the temperature anisotropy of ring current ions and subsequent nonlinear evolution (Shoji & Omura, 2011) are a process to generate plasmaspheric EMIC waves, and the EMIC waves propagate along the field line.

This nonlinear evolution of EMIC waves was confirmed by Akebono (Sakaguchi et al., 2013). Ion cyclotron whistlers are also EMIC mode waves that have been generated by lightning discharges through mode conversion (e.g., Gurnett et al., 1965; Matsuda et al., 2015). Recently, Horne and Miyoshi (2016) presented a theoretical analysis of the mode conversion that occurs between EN emissions and the proton band of EMIC waves. They predicted that mode conversion across different wave branches is possible if their propagation angles are parallel to the ambient magnetic fields.

In addition to these processes as an origin of the plasmaspheric EMIC waves, the conversion from EN emissions into oblique EMIC waves in the plasmasphere is shown in this study. When EN emissions propagate earthward across the field lines, the EN emissions convert into different wave modes; EN emission and EMIC waves occur with the presence of  $M/Q = 2$  ions in the deep plasmasphere and the topside ionosphere. Table 1 summarizes the origin of plasmaspheric EMIC waves. In this process, the presence of  $M/Q = 2$  ions plays an important role in controlling the conversion process. As shown in Figure 4, the composition ratio of  $M/Q = 2$  ions increases at the low altitudes, EMIC waves generated through the conversion from EN emission are mainly observed in the deep plasmasphere and in the topside ionosphere. The EMIC waves that were identified in this study showed oblique propagation because the seed EN emissions propagate across the field line, as shown in Figure 1, which is different from the propagation angle of EMIC waves through other generation processes.

**Table 1**  
Possible Origins of Plasmaspheric EMIC Waves

	Mechanisms	Frequency	Wave normal angle of EMIC waves	Reference
Direct generation	Cyclotron instability	A few hertz	Parallel propagation	Sakaguchi et al. (2013)
Parallel mode conversion	(a) Mode conversion from EN emissions across the different branches	A few tens hertz to multihundred hertz	Parallel propagation	(a) Horne and Miyoshi (2016)
	(b) Mode conversion from the lightning whistler across the different branches (ion cyclotron whistlers)			(b) Gurnett et al. (1965) and Matsuda et al. (2015)
Oblique mode conversion	Branch splitting of EN emissions under the presence of $M/Q = 2$ ions	A few tens hertz	Oblique propagation	This study

Note. EMIC = electromagnetic ion cyclotron; EN = equatorial noise.

We determined the ion composition ratios using crossover frequency and the cutoff frequency of the EN emissions and the EMIC waves. While several previous studies identified the existence of a variety of ion species by using wave dispersion with ion cyclotron whistlers (Watanabe & Ondoh, 1976; Matsuda et al., 2014b, 2015, 2016), this study is the first quantitative assessment of the ion composition ratio inside the plasmasphere. Matsuda et al. (2015) reported the spatial distributions of  $M/Q = 2$  ions from the Akebono observations and showed the presence of  $M/Q = 2$  ions above  $L = 1.5$ . As shown in Figures 3 and 4, we identified  $M/Q = 2$  ions at lower altitudes, even below 1,000 km, which have not been reported previously.

The estimated altitude dependence of the  $H^+$  and  $O^+$  ratio is similar to the International Reference Ionosphere (IRI) model. On the other hand,  $M/Q = 2$  ions, which are not included in the IRI model, can be estimated from the proposed approach. Therefore, the method that was established in this study is potentially a useful diagnostic tool to investigate the ion composition in the inner plasmasphere and in the topside ionosphere. It is not possible to distinguish between deuterium and alpha particles from the wave data that were used in this study. However, it is reasonable to conclude that the primary candidate of  $M/Q = 2$  ions is deuterium from Earth's atmosphere rather than alpha particles from the Sun. As shown in Figure 4, the ratio of  $M/Q = 2$  ions increases with decreasing altitudes, and the relative composition ratio increases up to 10% in the low altitude. Plasma density at the topside ionosphere (and even in the plasmasphere) is dominated by very cold ions and electrons ( $<1$  eV), while the kinetic energy of the solar wind at  $\sim 1$  AU is  $\sim 1$  keV. Further statistical investigation on the spatial distribution and geomagnetic activity dependence is essential to clarify the properties of  $M/Q = 2$  ions in the deep plasmasphere.

#### Acknowledgments

The Van Allen Probes data used in this study have been opened to the public from the University of Minnesota (<http://www.space.umn.edu/missions/rbspewf-home-university-of-minnesota/>). We acknowledge useful discussions with C. Klezving, Y. Kato, and D.-H. Lee. Science data of the ERG (Arase) satellite were obtained from the ERG Science Center operated by ISAS/JAXA and ISEE/Nagoya University (<https://ergsc.isee.nagoya-u.ac.jp/index.shtml.en>). In the present data, we use level 1-prime WFC version 7 data and level-2 MGF 64 Hz v01.01. The Arase satellite data will be publicly available via ERG Science Center on a project-agreed schedule. This study is supported by Grants-in-Aid for Scientific Research (14J02108, 15H05815, 16H06286, 16J02163, 17K05668, 17K14400, 17K14402 and 26800257) of Japan Society for the Promotion of Science (JSPS). This research was supported by the Natural Environment Research Council (NERC) Highlight Topic grants NE/P01738X/1 (Rad-Sat) and NE/R016038/1. This study was supported by JSPS Bilateral Open Partnership Joint Research Projects. We also acknowledge support from the MEYS LTAUSA17070 project and from the Czech Academy of Sciences through the JSPS-17-14 project and through the Praemium Academiae award.

#### References

- Boardsen, S. A., Gallagher, D. L., Gurnett, D. A., Peterson, W. K., & Green, J. L. (1992). Funnel-shaped, low-frequency equatorial waves. *Journal of Geophysical Research*, *97*, 14,967–14,976. <https://doi.org/10.1029/92JA00827>
- Boardsen, S. A., Hospodarsky, G. B., Kletzing, C. A., Engebretson, M. J., Pfaff, R. F., Wygant, J. R., et al. (2016). Survey of the frequency dependent latitudinal distribution of the fast magnetosonic wave mode from Van Allen Probes Electric and Magnetic Field Instrument and Integrated Science waveform receiver plasma wave analysis. *Journal of Geophysical Research: Space Physics*, *121*, 2902–2921. <https://doi.org/10.1002/2015JA021844>
- Fraser, B. J. (1985). Observations of ion cyclotron waves near synchronous orbit and on the ground. *Space Science Reviews*, *42*, 357.
- Gul'elmi, A. V., Klaine, B. I., & Potapov, A. S. (1975). Excitation of magnetosonic waves with discrete spectrum in the equatorial vicinity of the plasmopause. *Planetary and Space Science*, *23*, 279–286.
- Gurnett, D. A. (1976). Plasma wave interactions with energetic ions near the magnetic equator. *Journal of Geophysical Research*, *81*, 2765–2770.
- Gurnett, D. A., Shawhan, S. D., Brice, N. M., & Smith, R. L. (1965). Ion cyclotron whistlers. *Journal of Geophysical Research*, *75*, 1342–1344. <https://doi.org/10.1029/JA075i007p01342>
- Horne, R. B., & Miyoshi, Y. (2016). Propagation and linear mode conversion of magnetosonic and electromagnetic ion cyclotron waves in the radiation belts. *Geophysical Research Letters*, *43*, 10,034–10,039. <https://doi.org/10.1002/2016GL070216>
- Horne, R. B., & Throne, R. M. (1993). On the preferred source location for the convective amplification of ion cyclotron waves. *Journal of Geophysical Research*, *98*, 9233–9247.
- Horne, R. B., Wheeler, G. V., & Alleyne, H. S. C. K. (2000). Proton and electron heating by radially propagating fast magnetosonic waves. *Journal of Geophysical Research*, *105*, 27,597–27,610. <https://doi.org/10.1029/2000JA000018>
- Kasahara, Y., Kasaba, Y., Kojima, H., Yagitani, S., Ishisaka, K., Kumamoto, A., et al. (2018). The Plasma Wave Experiment (PWE) on board the Arase (ERG) satellite. *Earth, Planets, Space*, *70*(86). <https://doi.org/10.1186/s40623-018-0842-4>
- Kasahara, Y., Kenmochi, H., & Kimura, I. (1994). Propagation characteristics of the ELF emissions observed by the satellite Akebono in the magnetic equatorial region. *Radio Science*, *29*, 751–767. <https://doi.org/10.1029/94RS00445>
- Kasahara, Y., Sawada, A., Yamamoto, M., Kimura, I., Kokubun, S., & Hayashi, K. (1992). Ion cyclotron emissions observed by the satellite Akebono in the vicinity of the magnetic equator. *Radio Science*, *27*, 347–362. <https://doi.org/10.1029/91RS01872>
- Kimura, I. (1966). Effects of ions on whistler mode ray tracing. *Radio Science*, *1*. <https://doi.org/10.1002/rds196613269>
- Kletzing, C. A., Kurth, W. S., Acuna, M., MacDowall, R. J., Torbert, R. B., Averkamp, T., et al. (2013). The Electric and Magnetic Field Instrument Suite and Integrated Science (EMFISIS) on RBSP. *Space Science Reviews*, *179*, 127–181. <https://doi.org/10.1007/s11214-013-9993-6>
- Kurth, W. S., DePascuale, S., Kletzing, J. B. F. C. A., Hospodarsky, G. B., Thaller, S., & Wygant, J. R. (2015). Electron densities inferred from plasma wave spectra obtained by the Waves instrument on Van Allen Probes. *Journal of Geophysical Research: Space Physics*, *120*, 904–914. <https://doi.org/10.1002/2014JA020857>
- Ma, Q., Li, W., Chen, L., Thorne, R. M., & Angelopoulos, V. (2014). Magnetosonic wave excitation by ion ring distribution in the Earth's magnetosphere. *Journal of Geophysical Research: Space Physics*, *119*, 844–852. <https://doi.org/10.1002/2013JA019591>
- Ma, Q., Li, W., Chen, L., Thorne, R. M., Kletzing, C. A., Kurth, W. S., et al. (2014). The trapping of equatorial magnetosonic waves in the Earth's outer plasmasphere. *Geophysical Research Letters*, *41*, 6307–6313. <https://doi.org/10.1002/2014GL061414>
- Matsuda, S., Kasahara, Y., & Goto, Y. (2014a). Electromagnetic ion cyclotron waves suggesting minor ion existence in the inner magnetosphere observed by the Akebono satellite. *Journal of Geophysical Research: Space Physics*, *119*, 4348–4357. <https://doi.org/10.1002/2013JA019370>
- Matsuda, S., Kasahara, Y., & Goto, Y. (2014b). High-altitude  $M/Q = 2$  ion cyclotron whistler in the inner magnetosphere observed by the Akebono satellite. *Geophysical Research Letters*, *41*, 3759–3765. <https://doi.org/10.1002/2014GL060459>

- Matsuda, S., Kasahara, Y., & Goto, Y. (2015). M/Q = 2 ion distribution in the inner magnetosphere estimated from ion cyclotron whistler waves observed by the Akebono satellite. *Journal of Geophysical Research: Space Physics*, *120*, 2783–2795. <https://doi.org/10.1002/2014JA020972>
- Matsuda, S., Kasahara, Y., & Kletzing, C. A. (2016). Variation in crossover frequency of EMIC waves in plasmasphere estimated from ion cyclotron whistler waves observed by Van Allen Probe A. *Geophysical Research Letters*, *43*, 28–24. <https://doi.org/10.1002/2015GL066893>
- Matsuda, S., Kasahara, Y., Kojima, H., Kasaba, Y., Yagitani, S., Ozaki, M., et al. (2018). Onboard software of plasma wave experiment aboard Arase: Instrument management and signal processing of Waveform Capture/Onboard Frequency Analyzer. *Earth, Planet, Space*, *70*(75). <https://doi.org/10.1186/s40623-018-0838-0>
- Matsuda, S., Kasahara, Y., Miyoshi, Y., Nomura, R., Shoji, M., Matsuoka, A., et al. (2018). Spatial distribution of fine-structured and unstructured EMIC waves observed by the Arase satellite. *Geophysical Research Letters*, *45*, 11,530–11,538. <https://doi.org/10.1029/2018GL080109>
- Matsuoka, A., Teramoto, M., Nomura, R., Nose, M., Fujimoto, A., Tanaka, Y., et al. (2018). The Arase (ERG) magnetic field investigation. *Earth, Planets, Space*, *70*(43). <https://doi.org/10.1186/s40623-018-0800-1>
- Min, K., & Liu, K. (2015). Regime transition of ion Bernstein instability driven by ion shell velocity distributions. *Journal of Geophysical Research: Space Physics*, *120*, 8448–8454. <https://doi.org/10.1002/2015JA021514>
- Miyoshi, Y., Hori, T., Shoji, M., Teramoto, M., Chang, T.-F., Segawa, T., et al. (2018). The ERG Science Center. *Earth, Planets, Space*, *70*(96). <https://doi.org/10.1186/s40623-018-0867-8>
- Miyoshi, Y., Shinohara, I., Takashima, T., Asamura, K., Higashio, N., Mitani, T., et al. (2018). Geospace exploration project ERG. *Earth, Planets, Space*, *70*(101). <https://doi.org/10.1186/s40623-018-0862-0>
- Parrot, M., Santolik, O., & Nemeč, F. (2016). Chorus and chorus-like emissions seen by the ionospheric satellite DEMETER. *Journal of Geophysical Research: Space Physics*, *121*, 3781–3792. <https://doi.org/10.1002/2015JA022286>
- Rauch, J. L., & Roux, A. (1982). Ray tracing of ULF waves in a multicomponent magnetospheric plasma: Consequences for the generation mechanism of ion cyclotron waves. *Journal of Geophysical Research*, *87*(A10), 8191–8198. <https://doi.org/10.1029/JA087iA10p08191>
- Russell, C. T., Holzer, R. E., & Smith, E. J. (1970). OGO 3 observations of ELF noise in the magnetosphere. The nature of equatorial noise. *Journal of Geophysical Research*, *75*, 755–768.
- Sakaguchi, K., Kasahara, Y., Shoji, M., Omura, Y., Miyoshi, Y., Nagatsuma, T., et al. (2013). Akebono observations of EMIC waves in the slot region of the radiation belts. *Geophysical Research Letters*, *40*, 1–5. <https://doi.org/10.1002/2013GL058258>
- Santolik, O., & Gurnett, D. A. (2002). Propagation of auroral hiss at high altitudes. *Geophysical Research Letters*, *29*(10), 1481. <https://doi.org/10.1029/2001GL013666>
- Santolik, O., Nemeč, F., Gerenova, K., Macusova, E., de Conchy, Y., & Cornilleau-Wehrin, N. (2004). Systematic analysis of equatorial noise below the lower hybrid frequency. *Annals of Geophysics*, *22*, 2587–2595. <https://doi.org/10.5194/angeo-22-2587-2004>
- Santolik, O., & Parrot, M. (1999). Case studies on wave propagation and polarization of ELF emissions observed by Freja around the local proton gyro-frequency. *Journal of Geophysical Research*, *104*(A2), 2459–2475.
- Santolik, O., & Parrot, M. (2000). Application of wave distribution function methods to an ELF hiss event at high latitudes. *Journal of Geophysical Research*, *105*, 18,885–18,894.
- Santolik, O., Parrot, M., & Lefeuvre, F. (2003). Singular value decomposition methods for wave propagation analysis. *Radio Science*, *38*(1), 1010. <https://doi.org/10.1029/2000RS002523>
- Santolik, O., Parrot, M., & Nemeč, F. (2016). Propagation of equatorial noise to low altitudes: Decoupling from the magnetosonic mode. *Geophysical Research Letters*, *43*, 6694–6704. <https://doi.org/10.1002/2016GL069582>
- Sawada, A., Kasahara, Y., Yamamoto, M., & Kimura, I. (1991). ELF emissions observed by the EXOS-D satellite around the geomagnetic equatorial region. *Geophysical Research Letters*, *18*, 317–320.
- Shoji, M., Miyoshi, Y., Omura, Y., Kistler, L. M., Kasaba, Y., Matsuda, S., et al. (2018). Instantaneous frequency analysis on nonlinear EMIC emissions: Arase observation. *Geophysical Research Letters*, *45*, 13,199–13,205. <https://doi.org/10.1029/2018GL079765>
- Shoji, M., & Omura, Y. (2011). Simulation of electromagnetic ion cyclotron triggered emissions in the Earth's inner magnetosphere. *Journal of Geophysical Research*, *116*, A05212. <https://doi.org/10.1029/2010JA016351>
- Umeda, T., Matsukiyo, S., Amano, T., & Miyoshi, Y. (2012). A numerical electromagnetic linear dispersion relation for Maxwellian ring-beam velocity distributions. *Physics of Plasma*, *19*(7), 72,107. <https://doi.org/10.1063/1.4736848>
- Watanabe, S., & Ondoh, T. (1976). Deuteron whistler and trans-equatorial propagation of the ion cyclotron whistler. *Planetary and Space Science*, *24*, 359–364.
- Wygant, J. R., Bonnell, J. W., Goetz, K., Ergun, R. E., Mozer, F. S., Bale, S. D., et al. (2013). The electric field and waves instruments on the Radiation Belt Storm Probes Mission. *Space Science Reviews*, *179*(1–4), 183–220. <https://doi.org/10.1007/s11214-013-0013-7>
- Xiao, F., Zhou, Q., He, Y., Yang, C., Liu, S., Baker, D., et al. (2015). Penetration of magnetosonic waves into the plasmasphere observed by the Van Allen Probes. *Geophysical Research Letters*, *42*, 7287–7294. <https://doi.org/10.1002/2015GL065745>